



Contents lists available at ScienceDirect

Electrochimica Acta

journal homepage: www.elsevier.com/locate/electacta

Electrochemical properties of $\text{MmNi}_{3.03}\text{Si}_{0.85}\text{Co}_{0.60}\text{Mn}_{0.31}\text{Al}_{0.08}$ hydrogen storage alloys in alkaline electrolytes—A cyclic voltammetric study at different temperatures

M. Raju^a, M.V. Ananth^a, L. Vijayaraghavan^{b,*}^a Nickel–Metal Hydride Battery Section, Electrochemical Power Systems Division, Central Electrochemical Research Institute, Karaikudi 630006, India^b Manufacturing Engineering Section, Department of Mechanical Engineering, Indian Institute of Technology Madras, Chennai 600036, India

ARTICLE INFO

Article history:

Received 30 June 2008

Received in revised form 4 September 2008

Accepted 6 September 2008

Available online 13 September 2008

Keywords:

AB₅-type metal hydride alloy

Ni–MH battery

Cyclic voltammogram

Hydrogen diffusivity

Corrosion potential

ABSTRACT

The cyclic voltammetric behavior of $\text{MmNi}_{3.03}\text{Si}_{0.85}\text{Co}_{0.60}\text{Mn}_{0.31}\text{Al}_{0.08}$ -based metal hydride electrode was studied in alkaline electrolytes at various temperatures (303, 308, 318 and 328 K). Electrochemical parameters such as limiting current density and corrosion potential were determined at these temperatures. The corrosion potential became more negative with increasing temperature. Hydrogen diffusivity was also found to increase with increasing temperature. From electrochemical discharge experiments, it was concluded that the charge transfer process was the rate-determining step.

© 2008 Elsevier Ltd. All rights reserved.

1. Introduction

Nickel–metal hydride (Ni–MH) batteries are popular energy storage systems due to their inherent advantages such as high energy density, high-rate capability, environmental compatibility, etc. They also hold much promise for electric vehicle applications. The performance of the system relies on the electrochemical activity of a metal hydride alloy negative electrode, which replaces the toxic cadmium electrode employed in the conventional Ni–Cd cell. The Ni–MH battery employs different types of hydrogen storage intermetallic compounds (AB, AB₂, A₂B, AB₅, etc.) as negative electrode materials. The performance of the Ni–MH cell depends on the absorption and desorption of hydrogen during charging and discharging, respectively [1]. In the recent past, however, prospects for Ni–MH cells are beginning to be challenged by rapid developments in Li-ion battery technology. Currently, investigations on new types of alloy electrodes with higher capacity and longer cycle life are in progress in order to enhance the competitiveness of Ni–MH batteries in the rechargeable battery market.

Misch-metal-based AB₅-type alloys are among the most extensively investigated materials for use as anodes in Ni–MH batteries because of their low cost and availability [2,3]. They exhibit long

cycle life and superior performance compared to other competing materials. Misch-metal formulations with different permutations and combinations within permissible limits are possible, thereby enabling wide variations in their properties. Among the various factors that can influence the properties, La/Ce ratio is believed to have a significant role on electrochemical hydrogen storage. However, the available literature is scarce on studies on the effect of rare earth content on electrode performance [4,5]. Previous investigations in this laboratory demonstrated that the La/Ce ratio in the misch-metal had a decisive role in the electrochemical properties of the alloy [5]. Among the alloys studied by us, $\text{MmNi}_{3.03}\text{Si}_{0.85}\text{Co}_{0.60}\text{Mn}_{0.31}\text{Al}_{0.08}$ alloy with a La/Ce ratio of 11.65 in Mm exhibited the best performance.

The performance of metal hydride electrodes is dictated by the kinetics of the redox reactions occurring at the electrode–electrolyte interface during hydrogen absorption and desorption. The kinetic parameters of the redox reaction have been estimated by several electroanalytical techniques at room temperature [6–10]. However, electric vehicle and hybrid electric vehicle applications require fast charge–discharge and high-rate capability, which result in internal heat generation. High temperatures can be detrimental to the redox reactions, charge acceptance, specific capacity and cycle life of a battery. External heating or cooling will also affect battery performance and therefore necessitate proper thermal management. For electric vehicle applications, Ni–MH battery stacks must operate in a wide temperature range of 0–60 °C.

* Corresponding author. Tel.: +91 44 22574687; fax: +91 44 22570509.
E-mail address: lvijay@iitm.ac.in (L. Vijayaraghavan).

Thus, a study of the electrode kinetics of the processes at the MH electrode as a function of temperature is essential. In this paper, we present the results of our study on the performance of $\text{MmNi}_{3.03}\text{Si}_{0.85}\text{Co}_{0.60}\text{Mn}_{0.31}\text{Al}_{0.08}$ (the best performing alloy identified in our previous work [6]) at various temperatures (303, 308, 318 and 328 K).

2. Experimental

Non-stoichiometric lanthanum-rich AB₅-type rare earth metal-based hydride alloy powder ($\text{MmNi}_{3.03}\text{Si}_{0.85}\text{Co}_{0.60}\text{Mn}_{0.31}\text{Al}_{0.08}$) was used to prepare the negative electrode of the Ni–MH cell. The La/Ce ratio in Mm was 11.65. The purity of the constituent metals (La, Ce, Ni) was at least 99.9%. In order to ensure homogeneity, ingots were turned over and melted twice. The ingots were mechanically pulverized into fine powders of sieve size less than 75 μm . The composition of the product was determined by X-ray fluorescence spectroscopy (Horiba XRF analyzer, model XGT-2700).

Test electrodes for galvanostatic charge/discharge experiments were made from 1.00 g of the alloy and had a geometrical area of 3 cm \times 2 cm. Electrodes for cyclic voltammetry experiments were made with 0.17 g of the alloy and had a geometrical area of 1 cm \times 1 cm. A slurry of the alloy powder with 10% conducting material (carbon powder) and 5% binder (polytetrafluoroethylene) was prepared and subsequently applied to both sides of a nickel foam substrate, which was compacted and heat-treated at 408 K.

The test cell consisted of a three-electrode system in which the metal hydride alloy electrode acted as the working electrode, a sintered Ni(OH)₂ electrode (of higher capacity than the working electrode) as the counter electrode, and an Hg/HgO in 6 M KOH as the reference electrode. Galvanostatic charge/discharge cycling was carried out at a current density of 60 mA g⁻¹ on a Bitrode LCN life cycle tester. Charging was done for 7 h and discharging was done until the potential of the alloy electrode reached -0.7 V with respect to the reference electrode. After completion of the activation cycles, the temperature was raised using a water bath to 308, 318 or 328 K. At each temperature charge–discharge experiments were carried out at a constant current density of 60 mA g⁻¹ of the active material (C/5 rate). Cyclic voltammetric experiments were performed at room temperature (303 K) at 2, 5, 10, 20, and 50 mV s⁻¹ within the scanning potential range of -1.2 to -0.4 V with respect to the Hg/HgO reference electrode. Subsequently, the surrounding temperature was raised to 308, 318, and 328 K and cyclic voltammetric experiments performed as described for 303 K.

3. Results and discussion

The charging curves of the alloy electrode at 303, 308, 318 and 328 K performed at C/5 rate are shown in Fig. 1. It can be seen that the potential profile decreases suddenly and reaches a plateau region beyond 60 mA h g⁻¹. Furthermore, a decrease in the potential plateau is observed with increase in temperature. The charging profiles indicate phase transformations occurring during hydrogenation. The region A–B represents the α -phase, in which the hydrogen content is low, $x < 0.1$ H/M (H/M: hydrogen-to-metal ratio). At point B, the hydrogen content in the alloy becomes saturated. The hydrogen absorption/desorption in the single-phase solid solution in the gas-phase reaction can be described by the reaction:



From point B, upon hydrogenation the alloy undergoes transition to the metal hydride, or the β -phase. Also at B, the β -phase region starts i.e., α -phase and β -phase are present in the region

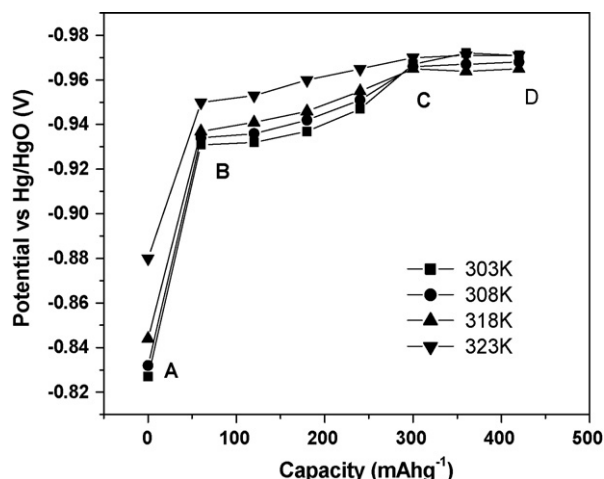
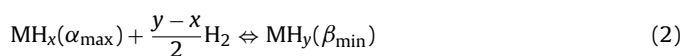


Fig. 1. Charge performance of $\text{MmNi}_{3.03}\text{Si}_{0.85}\text{Co}_{0.60}\text{Mn}_{0.31}\text{Al}_{0.08}$ alloy metal hydride electrode at various temperatures.

B–C. The region C–D is ascribed to hydrogen evolution. Hydrogen absorption reaches a saturation value at C. Any further charging leads to liberation of hydrogen at the negative electrode. The liberated hydrogen may take part in a recombination reaction with the oxygen liberated at the positive electrode. For $0.1 < x < 0.8$ H/M, i.e., from B \rightarrow C, there is a two-phase domain. Here, the saturated α -phase ($x = \alpha_{\text{max}}$) transforms into the β -phase ($x = \beta_{\text{min}}$), which corresponds to a plateau pressure. The compositional range of this plateau extends to as long as the following equilibrium reaction takes place:



A solid solution single-phase domain also exists at values of $x > 0.8$ H/M, which is a region corresponding to the β -phase close to point C. The single-phase domain can be described according to Eq. (1).

The discharge profiles depicted in Fig. 2 demonstrate that variation in temperature could significantly affect the performance of the alloy. It can be noted from the figure that the capacity decreases as the temperature is raised. The maximum discharge capacity was 281 mA h g⁻¹ at 303 K. The capacity decreased to 274, 245 and 229 mA h g⁻¹ at 308, 318 and 328 K, respectively. Moreover, at the highest temperature studied (328 K) the elec-

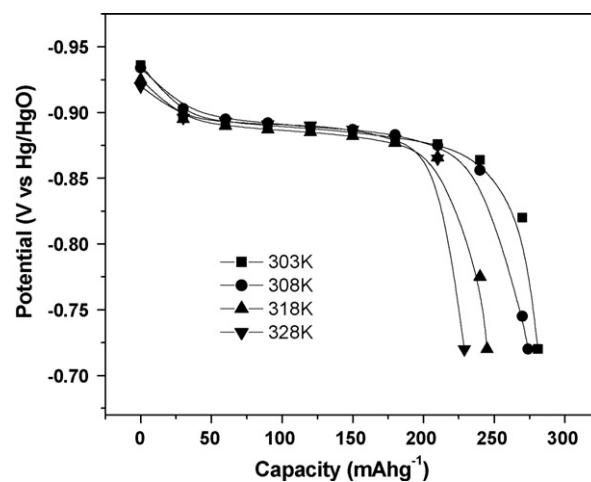


Fig. 2. Discharge performance of $\text{MmNi}_{3.03}\text{Si}_{0.85}\text{Co}_{0.60}\text{Mn}_{0.31}\text{Al}_{0.08}$ alloy metal hydride electrode at various temperatures.

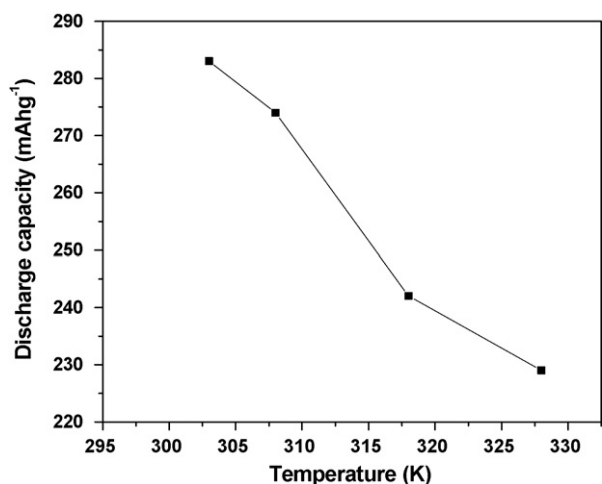


Fig. 3. Specific capacity of $\text{MmNi}_{3.03}\text{Si}_{0.85}\text{Co}_{0.60}\text{Mn}_{0.31}\text{Al}_{0.08}$ alloy metal hydride electrode as a function of temperature.

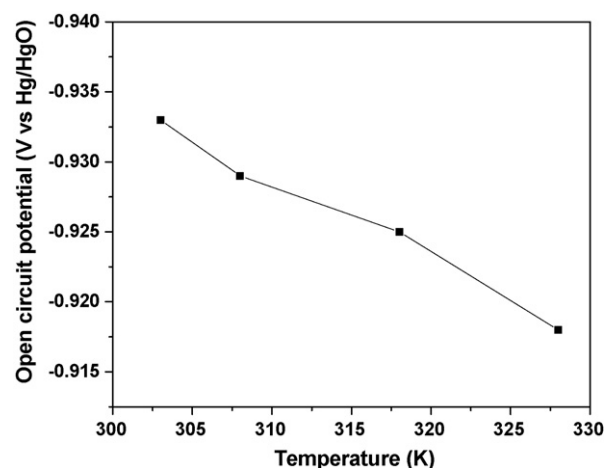


Fig. 4. Influence of temperature on open-circuit potential of $\text{MmNi}_{3.03}\text{Si}_{0.85}\text{Co}_{0.60}\text{Mn}_{0.31}\text{Al}_{0.08}$ alloy metal hydride electrode.

trode potential reaches a maximum value and exhibits the highest capacity fade too. This may be due to two important reactions involved in the metal hydride electrodes: increased rates of charge transfer and mass transfer reactions with increasing temperature. However, an increase in temperature results in a diminution of discharge capacity that can be related to enhanced hydrogen evolution (self-discharge) at elevated temperatures. Consequently, hydrogen adsorption in the electrode decreases and results in decreased capacity.

Charge transfer processes control the redox reactions at the electrode–electrolyte interface while mass transfer processes control those in the bulk. Variation in the specific capacity as a

function of temperature is illustrated in Fig. 3. As observed earlier, an increase in temperature leads to decrease in hydrogen storage capacity. The loss in capacity may also be due to accelerated self-discharge (poor charge retention) and increase in the equilibrium pressure at elevated temperatures. Fig. 4 illustrates the dependence of the open-circuit potential on temperature. The decrease in open-circuit potential with increasing temperature could be attributed to acceleration in the rate of the hydrogen evolution reaction.

Capacity loss at higher temperatures can also be related to the formation upon discharge of the γ -phase of nickel hydroxide, which is considered undesirable due to its relatively higher

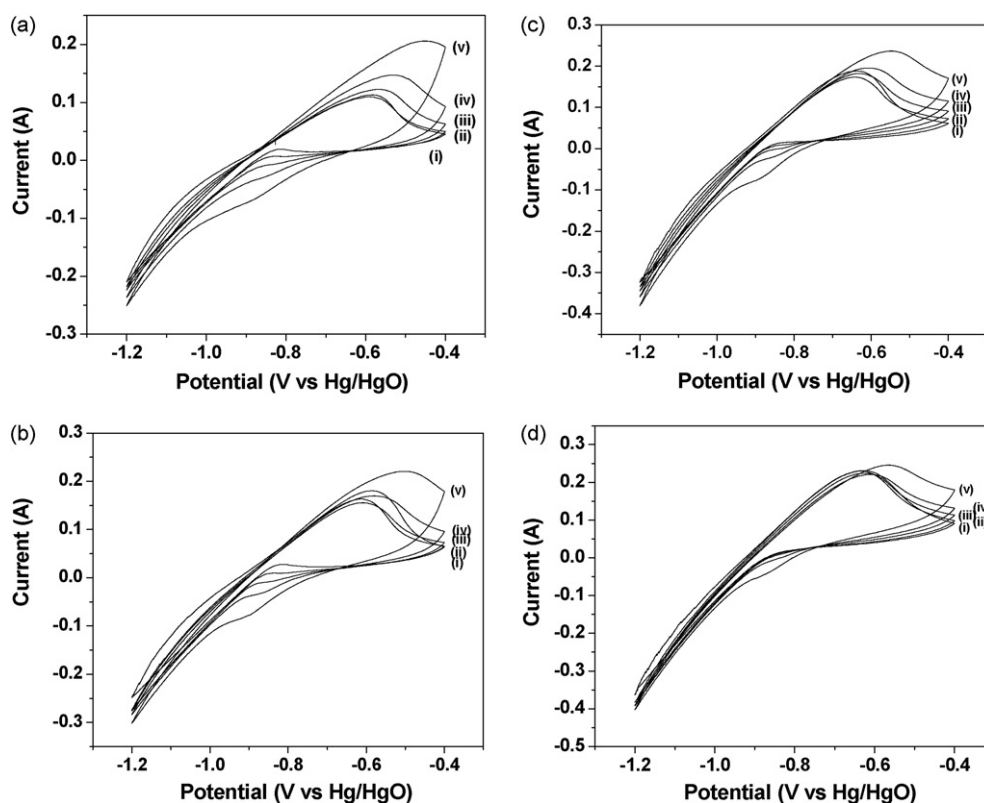


Fig. 5. Cyclic voltammograms of $\text{MmNi}_{3.03}\text{Si}_{0.85}\text{Co}_{0.60}\text{Mn}_{0.31}\text{Al}_{0.08}$ alloy metal hydride electrode at various temperatures. (a) 303 K, (b) 308 K, (c) 318 K, and (d) 328 K. (i) 2 mVs^{-1} , (ii) 5 mVs^{-1} , (iii) 10 mVs^{-1} , (iv) 20 mVs^{-1} , and (v) 50 mVs^{-1} .

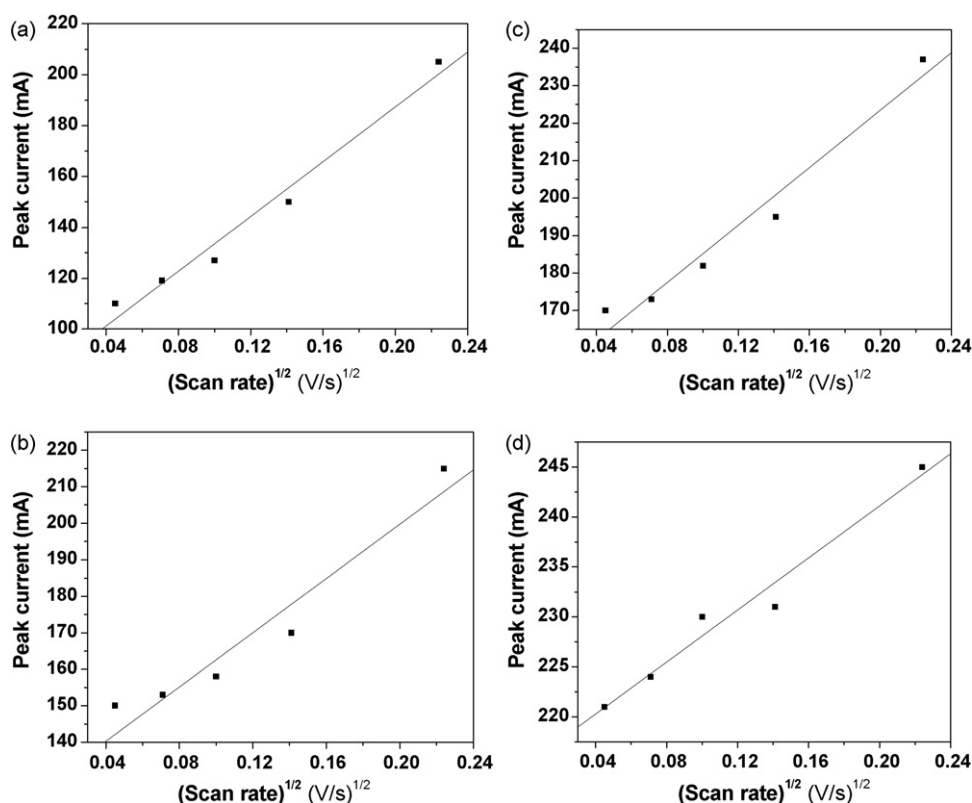


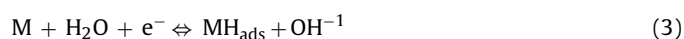
Fig. 6. Peak currents of cyclic voltammograms as a function of square root of scan rate for MmNi_{3.03}Si_{0.85}Co_{0.60}Mn_{0.31}Al_{0.08} alloy metal hydride electrode. (a) 303 K, (b) 308 K, (c) 318 K, (d) 328 K.

unit cell volume compared to that of the β -phase nickel hydroxide. The increased volume changes during charge–discharge due to the formation of the γ -phase that disrupts the conductive pathway between the nickel hydroxide particles and the substrate. The γ -phase nickel hydroxide consumes water, which forms when percolating oxygen molecules combine with hydrogen in the metal hydride. During this process, a redistribution of electrolyte occurs, which might lead to oxidation of the hydrogen storage materials and lowering of cell voltage. The presence of the γ -phase is also detrimental to capacity retention, thereby reducing the charge reserve in the negative electrode.

The cyclic voltammograms recorded with the alloy electrode at scan rates between 2 and 50 mV s⁻¹ at various temperatures (303, 308, 318, and 328 K) are depicted in Fig. 5a–d. At all the temperatures, a large, broad peak is seen around -0.6 V, which is attributed to mass transfer and charge transfer of absorbed hydrogen in the bulk and adsorbed hydrogen at the electrode surface. The small, broad peak at -0.9 V observed in the anodic scan at all temperatures, especially with the cyclic voltammograms recorded at 20 and 50 mV s⁻¹, indicates a higher charging capacity, i.e., a larger concentration of hydrogen in the electrode. Below -0.9 V, the current rapidly increases in the negative direction, a phenomenon influenced by the hydrogen evolution reaction. It can be noted that an increase in the scan rate shifts the peak potential in the positive direction. The peak current also increases with scan rate and temperature. The anodic polarization current for the charged metal hydride electrode involves hydrogen charge transfer reactions across the electrode–electrolyte interface. This process also involves hydrogen diffusion in the alloy powder. At low scan rates, hydrogen in the interior of the alloy has sufficient time to diffuse into the powder surface. The diffused hydrogen at the surface also participates in the charge transfer reaction.

Generally, the anodic current increases with scan rate. At higher temperatures the thickness of the diffusion layer decreases, which facilitates a fast release of hydrogen from the surface layer, leading to a rapid increase in the anodic current. At scan rates of 20 and 50 mV s⁻¹, the limiting current varies linearly with the square root of the scan rate. The relationship between peak current, I_p , and square root of scan rate is described in Fig. 6a–d. Furthermore, the peak potential is also proportional to the square root of the scan rate (Figs. 3 and 4). Hence, it can be concluded that the metal hydride electrode is not a totally reversible system, and that within the scan range employed in this study charge transfer is the rate-determining step in the electrode reaction [11].

The primary electrochemical reactions that occur at the metal hydride electrode are



where M is the hydrogen storage alloy, H_{ads} the adsorbed hydrogen on the surface of the alloy, H_{abs} the adsorbed hydrogen in the bulk, and H_{hyd} is the metal hydride [12]. During charging, hydrogen is adsorbed on the electrode surface, which subsequently gets absorbed into the bulk by diffusion before finally forming the metal hydride (Eqs. (3)–(5)). Generally, the relative rates of the individual reactions and especially the coulombic efficiency of hydrogen entry and withdrawal in metal hydride systems strongly depend on the magnitude of the metal–hydrogen interactive energy, which in turn depends on temperature. The electro-reduction of water molecules becomes slower whereas the rate of hydrogen evolution increases. Hydrogen diffusion in a charge–discharge reaction is influenced both by the micro- and macro-structures of the alloy.

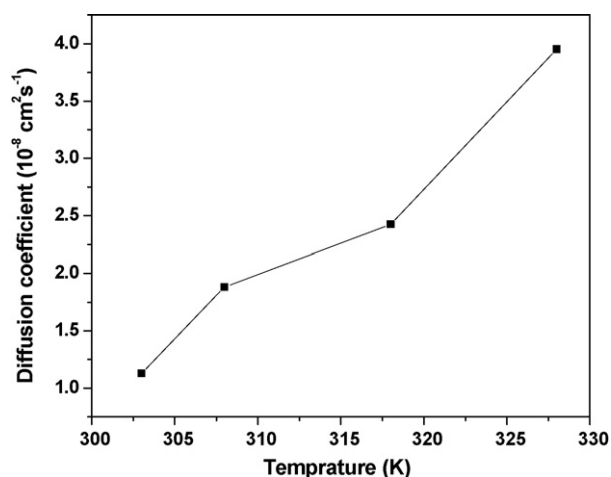


Fig. 7. Diffusion coefficient of $\text{MmNi}_{3.03}\text{Si}_{0.85}\text{Co}_{0.60}\text{Mn}_{0.31}\text{Al}_{0.08}$ alloy metal hydride electrode as a function of temperature.

The diffusion coefficient of atomic hydrogen in the solid phase was shown to depend on the metal–hydrogen interaction and the concentration of hydrogen in the bulk. In fact, these are characteristics of mass transport in metal hydride electrodes [12]. Hence, it is clear from Eqs. (3) and (4) that the kinetics of hydrogenation at the electrode/electrolyte interface is not only controlled by the charge transfer reaction but also by the hydrogen diffusivity into the bulk of the alloy particles. For electric vehicle and hybrid electric vehicle applications, the rate of diffusion is an important parameter for hydrogen storage alloys. An alloy with high diffusion coefficient would allow for transport of adsorbed hydrogen at the active surface site to the reaction zone during charging. Fast diffusion is an important factor when it comes to minimizing the rate of hydrogen evolution during charging [13].

Accordingly, the hydrogen diffusion coefficient, D , of the metal hydride electrode is evaluated from the following equation [11]:

$$I_p = 2.99 \times 10^5 n(\alpha n_\alpha)^{1/2} S C \nu^{1/2} D^{1/2} \quad (6)$$

where I_p is the peak current (A), n the charge transfer number, n_α the number of electrons transferred up to and including the rate-determining step, α the transfer coefficient, S the surface area (cm^2), C the concentration of the diffusion species (mol cm^{-3}), and ν the potential scan rate (V s^{-1}). The values of diffusion coefficient values at 303, 308, 318 and 328 K are 1.1289×10^{-8} , 1.8831×10^{-8} , 2.4253×10^{-8} and $3.9518 \times 10^{-8} \text{ cm}^2 \text{ s}^{-1}$, respectively (Fig. 7). This is comparable to the results of Yuan and Xu [11] for rare earth-based metal hydride alloys in the fully charged state. Various authors [12–17] have reported values of hydrogen diffusion coefficient between 10^{-6} and $10^{-11} \text{ cm}^2 \text{ s}^{-1}$ for metal hydride alloys, which agree with our results. Such wide variations in the values for the diffusion coefficient for similar types of alloys could be attributed to variations in the microstructure of the alloys. The microstructure of the alloys depends on their preparation and hydrogenation. The hydrogen diffusion coefficient can also vary with the type of hydrogenation process, i.e., gas-phase hydrogenation/electrochemical hydrogenation [18]. The value of the hydrogen diffusion coefficient increases with temperature, suggesting faster hydrogen diffusion at elevated temperatures. Hydrogen must transform from its absorbed state to the adsorbed state (structural transformation of MH alloy from β to α) before diffusion. The increase in temperature facilitates the structural transformation and increases the hydrogen diffusion.

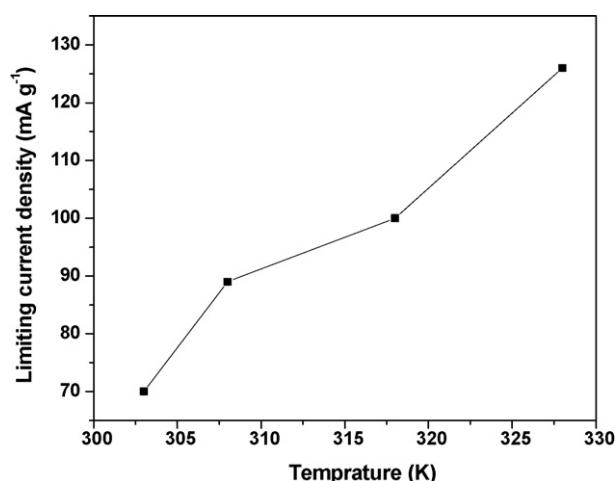


Fig. 8. Limiting current density of $\text{MmNi}_{3.03}\text{Si}_{0.85}\text{Co}_{0.60}\text{Mn}_{0.31}\text{Al}_{0.08}$ alloy metal hydride electrode as a function of temperature.

The limiting current for the irreversible charge transfer reaction can be expressed as [19]

$$i_L = 0.4958 n F A C_0 \left(\frac{\alpha n F}{RT} \right)^{1/2} D^{1/2} \nu^{1/2} \quad (7)$$

where ν is the scan rate in V s^{-1} , C_0 the initial hydrogen concentration in mol cm^{-3} , i_L the limiting current in A g^{-1} , D the hydrogen diffusion coefficient in $\text{cm}^2 \text{ s}^{-1}$, F the Faraday, A the surface area, R the gas constant, and T is the temperature. From the equation it can be seen that the limiting current density is strongly controlled by the hydrogen diffusion in the bulk of the alloy. The evaluated limiting current densities (Fig. 8) for the samples are 70.0, 89.0, 100.2 and 126.1 mA g^{-1} at 303, 308, 318 and 328 K, respectively. It is clear that the limiting current density increases with temperature, suggesting enhanced electrocatalytic activity at higher temperatures. Both hydrogen diffusion coefficient and limiting current density also increase as a function of temperature (Figs. 5 and 6). Thus, the higher the rate of hydrogen diffusion into the bulk, the larger is the limiting current density [20].

The three components of the discharge coulombic capacity (Q) of metal hydride electrodes obtained electrochemically as a function of applied potential scan rate in the cyclic voltammograms can be expressed as follows [21]:

$$Q(\nu) = Q_C(\nu) + Q_A(\nu) + Q_S \quad (8)$$

$$Q_S = n F A \Gamma \quad (9)$$

where Q_C corresponds to the release of absorbed hydrogen from the alloy, Q_A corresponds to the activation polarization reaction, Q_S corresponds to the hydrogen surface coverage and surface area, A is the reaction surface area of the electrode and Γ is the hydrogen surface coverage. The discharge coulombic capacity obtained from cyclic voltammetry can be separated from the scan rate-dependent activation and concentration capacities (Q_C and Q_A) and the scan rate independent capacity (Q_S). The discharge coulombic capacity obtained electrochemically as a function of applied potential scan rate is shown in Fig. 9. The data is obtained at low scan rates and the current density observed is due to concentration polarization. The capacity, Q_C , in this case is related to the release of the absorbed hydrogen from the alloy. Due to concentration polarization hydrogen is released from the alloy. The rate of release increases with temperature. Capacity, Q_A , is lower due to activation polarization and is influenced at high scan rates. Q_S , the capacity due to hydrogen surface coverage (obtainable from the Y intercept) is negligible in

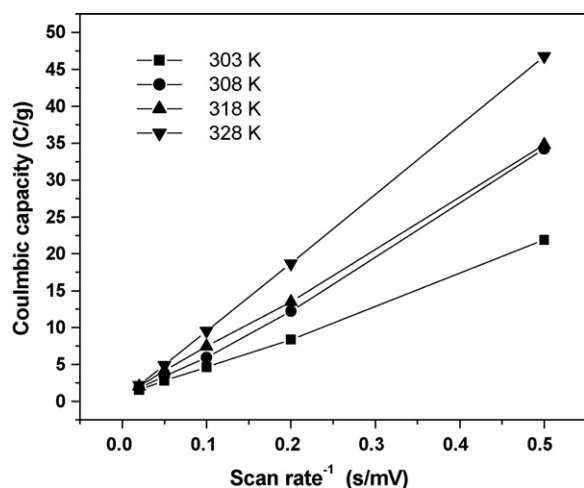


Fig. 9. Coulombic capacity of $\text{MmNi}_{3.03}\text{Si}_{0.85}\text{Co}_{0.60}\text{Mn}_{0.31}\text{Al}_{0.08}$ alloy metal hydride electrode as a function of scan rate.

the present case. This may be due to the fact that hydrogen escapes at elevated temperatures instead of getting adsorbed into the alloy.

Temperature is one of the most critical parameters in corrosion studies. It affects the physico-chemical and electrochemical hydrogen absorption/desorption reaction rates. The corrosion of metal hydride electrode not only affects the hydrogen absorption capability but also the hydrogenation/dehydrogenation kinetics. Variation in corrosion potential as a function of potential scan rate at 303, 308, 318 and 328 K is shown in Fig. 10. Corrosion potential is the potential of the electrode at which the anodic and cathodic reactions are in dynamic equilibrium. This corresponds to the potential at the point of intersection of the anodic and cathodic curves in Tafel plots. The corrosion potential was obtained from the cyclic voltammetric data by using Autolab's General Purpose Electrochemical System (GPES) Tafel slope analysis software (Eco Chimie). A typical Tafel plot for the sample at 303 K and at a scan rate of 2 mV s^{-1} is shown in Fig. 11. The corrosion potential at low scan rates (2 and 5 mV s^{-1}) remains almost constant. However, at 10 , 20 and 50 mV s^{-1} , the corrosion potential becomes more negative and increases linearly with temperature. Since the temperature is a critical factor in the kinetics of chemical reactions, it could be concluded that the metal hydride alloy is more susceptible to corrosion at elevated temperatures in the alkaline environment.

Apart from the primary electrochemical reactions (Eqs. (3)–(5)), other electrochemical reactions such as gas recombination, overcharge and overdischarge reactions also occur in parallel. Moreover, it is believed that capacity degradation in Ni–MH batteries is

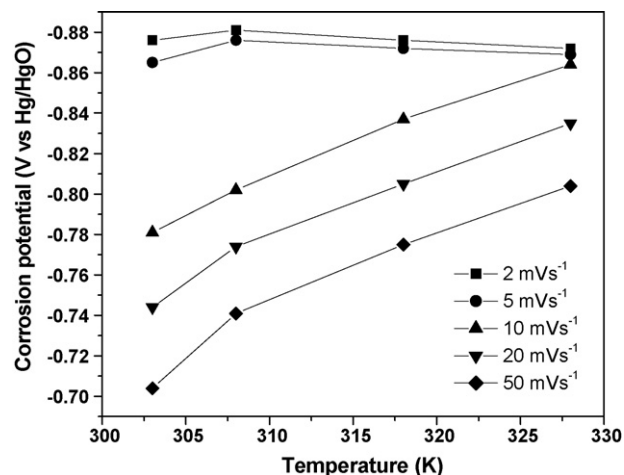


Fig. 10. Corrosion potential of $\text{MmNi}_{3.03}\text{Si}_{0.85}\text{Co}_{0.60}\text{Mn}_{0.31}\text{Al}_{0.08}$ alloy metal hydride electrode as a function of temperature at different potential scan rates.

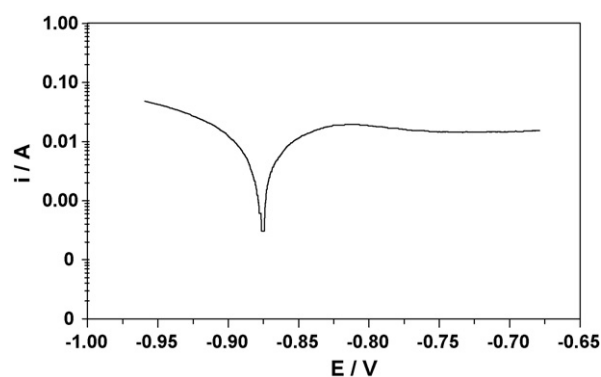


Fig. 11. A typical Tafel plot for $\text{MmNi}_{3.03}\text{Si}_{0.85}\text{Co}_{0.60}\text{Mn}_{0.31}\text{Al}_{0.08}$ alloy metal hydride electrode at 303 K and at a scan rate of 2 mV s^{-1} .

due to self-discharge during retention (i.e., self-discharge under open-circuit conditions). At elevated temperatures, the rate of the self-discharge reactions and the corroding tendency of the electrodes also increase, adversely affecting the hydrogen storage capacity. The single-phase alloy could also deteriorate at elevated temperatures. The alloy particles also get pulverized as the hydrogenation/dehydrogenation proceeds, as is evident from Fig. 12. Aluminum and manganese present in the alloy can limit alloy pulverization and oxidation. However, these metallic constituents being unstable in the alkaline environment get depleted during repeated cycling. During repeated charge–discharge, the metals

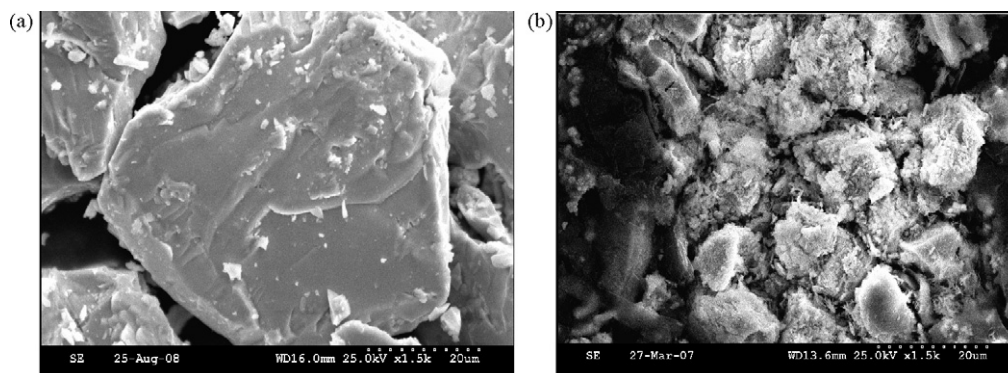


Fig. 12. Microstructure of $\text{MmNi}_{3.03}\text{Si}_{0.85}\text{Co}_{0.60}\text{Mn}_{0.31}\text{Al}_{0.08}$ alloy: (a) bare alloy particle and (b) pulverized alloy particle after 300th charge–discharge cycle.

get deposited on the positive electrode instead of performing their intended function in the negative electrode [22]. Because of pulverization (as seen from SEM results that the original alloy particles of size above 50 μm are reduced in size to 8 μm upon cycling), more fresh surface areas are created. The presence of soluble as well as insoluble corrosion products [4] over the new surfaces clog the conductive pathways between alloy particles, leading to degradation in capacity. These are among possible factors contributing to reduced capacity at elevated temperatures.

4. Conclusions

Electrokinetic properties of $\text{MmNi}_{3.03}\text{Si}_{0.85}\text{Co}_{0.60}\text{Mn}_{0.31}\text{Al}_{0.08}$ alloy were investigated by cyclic voltammetry between 303 and 328 K and galvanostatic charge/discharge at C/5 rate. Cyclic voltammetric results showed that the peak current increased with temperature and scan rate. Electrochemical discharge experiments revealed that the charge transfer was the rate-determining step. The coulombic capacity was found to decrease with temperature, which was attributed to concentration polarization. Hydrogen diffusion in the bulk alloy limits the discharge capability of the alloy. However, hydrogen diffusion coefficient increases with temperature. Charge–discharge studies showed that high temperatures adversely affected battery performance: both the open-circuit potential and discharge capacity decreased with increasing temperature, and the electrode became more susceptible to corrosion at elevated temperatures.

Acknowledgements

The authors thank the Director, CECRI for his encouragement and permission to publish this work. Thanks are also due to Dr.

N.G. Renganathan and Dr. M. Ganesan of the Electrochemical Power Systems Division, CECRI and Dr. G. Balachandran of the Rare Earth Processing Group, DMRL, Hyderabad for discussions and for preparing the alloy, respectively.

References

- [1] J. Kleperis, F. Wojcik, A. Czerwinski, J. Skowronski, M. Kopczyk, M. Beltowska-Brzenska, J. Solid State Electrochem. 5 (2001) 229.
- [2] M. Tliha, H. Mathlouthi, J. Lamloumi, A. Percheron-Guegan, J. Alloy Compd. 436 (2007) 221.
- [3] H. Ye, B. Xia, W.Q. Wu, K.D.H. Zhang, J. Power Sources 111 (2002) 145.
- [4] F. Maurel, B. Knosp, M. Backhaus-Ricoult, J. Electrochem. Soc. 147 (2000) 78.
- [5] M.V. Ananth, M. Raju, K. Manimaran, G. Balachandran, L.M. Nair, J. Power Sources 167 (2007) 228.
- [6] M. Tliha, M. Mathlouthi, J. Lamloumi, A. Percheron-Guegan, Int. J. Hydrogen Energ. 32 (2007) 611.
- [7] M. Raju, K. Manimaran, M.V. Ananth, N.G. Renganathan, Int. J. Hydrogen Energ. 32 (2007) 1721.
- [8] F. Feng, D.O. Northwood, Int. J. Hydrogen Energ. 29 (2004) 955.
- [9] W.X. Chen, J. Power Sources 90 (2000) 201.
- [10] X.F. Li, H.C. Dong, A.Q. Zhang, Y.W. Wei, J. Alloy Compd. 426 (2006) 93.
- [11] X.X. Yuan, N.X. Xu, J. Alloy Compd. 316 (2001) 113.
- [12] G. Zheng, B.N. Popov, R.E. White, J. Electrochem. Soc. 143 (1996) 834.
- [13] M. Mohamedi, T. Sato, T. Itob, M. Umeda, I. Uchida, J. Electrochem. Soc. 149 (2002) A983.
- [14] P. Fischer, A. Furrer, G. Busch, L. Schlappbach, Helv. Phys. Acta 50 (1977) 421.
- [15] T. Nishina, H. Ura, I. Uchida, J. Electrochem. Soc. 144 (1997) 1273.
- [16] C. Cai, D. Shao, B. Wang, Chin. J. Power Sources 17 (1993) 9.
- [17] J. Chen, S.X. Dou, D.H. Bradhurst, H.K. Liu, Int. J. Hydrogen Energ. 23 (1998) 177.
- [18] X.X. Yuan, N.X. Xu, J. Alloy Compd. 329 (2001) 115.
- [19] M. Geng, F. Feng, P.J. Sebastian, A. Matchett, D.O. Northwood, Int. J. Hydrogen Energ. 26 (2000) 165.
- [20] B.V. Ratnakumar, C. Witham, R.C. Bowman, A. Hightower, B. Fultz, J. Electrochem. Soc. 143 (1996) 2578.
- [21] S.A. Gamboa, P.J. Sebastian, F. Feng, M. Geng, D.O. Northwood, J. Electrochem. Soc. 149 (2002) A137.
- [22] P. Bernard, J. Electrochem. Soc. 145 (1998) 456.